



AgNPs/GO nanomaterial by a simple method and studied its antibacterial properties

Anabel Herrera-Rodríguez¹ · R. Esparza² · Juan Carlos González-Hernández³ · G. Rosas¹

Received: 27 June 2023 / Accepted: 31 October 2023 / Published online: 21 November 2023
© The Author(s), under exclusive licence to Springer-Verlag GmbH, DE part of Springer Nature 2023

Abstract

This study used the *Tamarix gallica* aqueous extract to simultaneously reduce silver ions and graphene oxide (GO), forming the AgNPs/GO nanocomposite in a single step. The agar diffusion method determines the material's antibacterial activity and tests its effectiveness against Gram-negative *Escherichia coli* ATCC 25922 and Gram-positive *Staphylococcus aureus* ATCC 29213. The properties of products were analyzed using various methods such as UV–Vis, SEM, XRD, STEM, and FT-IR to determine their morphology, structure, and chemical composition. XRD, SEM, and STEM analysis revealed that silver nanoparticles (AgNPs) were deposited on reduced graphene oxide (rGO). The AgNPs were semi-spherical in shape and had a face-centered cubic crystal structure with a size ranging from 5 to 40 nm. AgNPs/GO is antibacterial and effective against *Escherichia coli* and *Staphylococcus aureus*. However, Ag/rGO was more effective against *Staphylococcus aureus*.

Keywords AgNPs/GO nanocomposite · Green synthesis · *Tamarix gallica* · Antibacterial activity · *Escherichia coli* · *Staphylococcus aureus*

1 Introduction

Graphene, a two-dimensional layer of sp² hybridized carbon atoms arranged in a hexagonal lattice structure, has caught the attention of researchers since its discovery [1]. Its exceptional mechanical, electrical, thermal, and chemical properties have led to the development of new materials [2].

Graphene is the thinnest and strongest material and has two major derivatives: graphene oxide (GO) and reduced graphene oxide (rGO) [3]. GO is created by oxidizing and exfoliating graphite, resulting in a structure with many oxygenated functional groups [3]. At the same time, reducing GO to rGO decreases its functionalization [3]. Graphene and its derivatives are available materials as nanocomposites, improving the characteristics and performance [4]. These nanomaterials have applications in drug delivery, shape memory polymers, gene delivery, biosensors, tissue engineering, flexible electronic devices, antibacterial, photovoltaic devices, and physical sensors due to their exceptional mechanical and electrical, physical, and chemical properties [5]. Nanocomposites are produced by combining the bactericide action of inorganic nanoparticles with graphene-based nanomaterials to achieve synergistic effects [6]. Metal nanoparticles like copper (Cu), titanium (Ti), silver (Ag), gold (Au), and zinc (Zn) have long been used for their antimicrobial properties with broad activity spectra [7]. Among them, silver nanoparticles (AgNPs) are the most effective in inhibiting Gram-positive and Gram-negative bacteria growth [8, 9].

Different reducing agents have been utilized in synthesizing Ag/rGO nanocomposites through several chemical methods. For instance, Li et al. [10] used potassium hydroxide (KOH) and sodium hydroxide (NaOH) to

✉ G. Rosas
grtrejo07@yahoo.com.mx; grtrejo@umich.mx

Anabel Herrera-Rodríguez
anabel.herrera.rodriguez@umich.mx

R. Esparza
resparza@fata.unam.mx

Juan Carlos González-Hernández
juan.gh@morelia.tecnm.mx

¹ Instituto de Investigaciones en Metalurgia y Materiales, UMSNH Edificio U., Ciudad Universitaria, 58000 Morelia, Michoacán, Mexico

² Centro de Física Aplicada y Tecnología Avanzada CFATA-UNAM, 76230 Santiago de Querétaro, Querétaro, Mexico

³ Tecnológico Nacional de México/Instituto Tecnológico Morelia. Av. Tecnológico, 1500. Lomas de Santiaguillo, 58120 Morelia, Michoacán, Mexico

achieve their synthesis through microwave-assisted irradiation. Similarly, He et al. [11] utilized a two-step route involving chelating AgNPs onto GO in the presence of N, N-dimethylformamide, followed by sodium borohydride (NaBH_4) reduction. They demonstrated that this nanomaterial exhibits good chemical catalytic behavior towards reducing methylene blue and high electrocatalytic activity towards the electrooxidation of hydrazine. On the other hand, Çiplak [12] used sequential reduction of GO and AgNO_3 with hydrazine hydrate (N_2H_4) to obtain Ag/GO and Ag/rGO nanocomposites. They varied the amount and concentration of precursor salt and reducing agent. However, none of these works have been used for antibacterial applications due to the toxicity of the reducing agents to humans.

Using plant extracts as reducing and stabilizing agents in green methods has several advantages over other methods. These advantages include low cost, fast results, the ability to produce unlimited sizes and forms, and a simple scaling process [13, 14]. In one study, Veisi et al. [15] biosynthesized a nanocomposite using *Pistacia atlantica* leaf extract and tested its antibacterial activity against several bacteria. Similarly, Soleymani et al. [16] obtained nanohybrids through micro-fluidization using celery seed extract as a reducing green agent. This nanohybrid exhibited excellent antibacterial activity against Gram-positive and Gram-negative bacteria. Cobos et al. [17] also biosynthesized Ag/rGO nanocomposites using L-ascorbic acid as a reducing agent. They found that it had antimicrobial properties against Gram-negative *Escherichia coli*, Gram-negative *Pseudomonas aeruginosa*, Gram-positive *Staphylococcus aureus*, and the yeast *Candida albicans* dependent on the nanocomposite concentration and exposition time.

This research presents a new method for producing Ag/rGO nanocomposite using *Tamarix gallica* aqueous extract as a reducing and stabilizing agent. The process involves the simultaneous reduction of GO and Ag. We tested the antimicrobial properties of the nanomaterial against *Escherichia coli* ATCC 25922 and *Staphylococcus aureus* ATCC 29213 strains. It is worth noting that our workgroup had previously biosynthesized AgNPs with *Tamarix gallica* [18]. Ksouri et al. [19] found that *Tamarix gallica* contains various phenolic acids such as gallic, sinapic, chlorogenic, syringic, vanillic, p-coumaric, and trans-cinnamic. The flower extract of *Tamarix gallica* also contains six flavonoids, namely (+)-catechin, isoquercetin, quercetin, apigenin, amentoflavone, and flavone. On the other hand, the aqueous leave extract of *Tamarix gallica* contains twelve phenolic compounds, including gallic, sinapic, chlorogenic, syringic, vanillic, rosmarinic, p-coumaric, ferulic, and trans-cinnamic acids, and two flavonoids, namely quercetin, and amentoflavone.

2 Materials and methods

2.1 Materials

Carbon graphite powder (carbon > 99%), silver nitrate (AgNO_3 , 98%), and erythromycin hydrate ($\text{C}_{37}\text{H}_{67}\text{NO}_{13}\cdot x\text{H}_2\text{O}$, 96%) were acquired from Sigma-Aldrich. Sulfuric acid (H_2SO_4 , 95–98%), phosphoric acid (H_3PO_4 , $\geq 85\%$), potassium permanganate (KMnO_4 , $\geq 99.0\%$), hydrogen peroxide (H_2O_2 , 30 wt.%), ethyl alcohol ($\text{C}_2\text{H}_6\text{O}$, $\geq 99.5\%$), hydrochloric acid (HCl, 37 wt. %) and ethyl ether ($\text{C}_4\text{H}_{10}\text{O}$, $\geq 99.5\%$) were obtained from Meyer.

2.2 Graphene oxide preparation

The Hummers method modified by Marcano et al. [20] was used to obtain the graphite oxide. Initially, 1.8 g of KMnO_4 was slowly added in six equal portions to a 9:1 mixture of H_2SO_4 – H_3PO_4 (36:4 mL) and 0.3 g of graphite powder. Subsequently, the reaction was heated to 50 °C with constant magnetic stirring for 12 h. It was cooled to room temperature and poured onto ice (40 mL) with 30% H_2O_2 (0.3 mL). H_2O_2 is responsible for removing excess permanganate and manganese dioxide. Subsequently, the solution was centrifuged at 4000 rpm for 4 h. The solid was washed successively, first using 20 mL of water, second with 20 mL of 30% HCl, and twice with 20 mL of ethanol. The material obtained was coagulated in 20 mL of ether, and the resulting suspension was filtered through a Whatman No. 42 membrane, allowing it to dry in an oven overnight at 50 °C. The graphite oxide obtained was exfoliated in an ultrasound bath Branson model 1510 at a 0.08 mg/mL concentration for 25 min.

2.3 Preparation of *Tamarix gallica* aqueous

To prepare the *Tamarix gallica* aqueous extract, we took 1 g of dried plant (leaves and flowers), crushed it, and mixed it with 50 mL of deionized water. We stirred the mixture at 60 °C for 20 min using a Thermo Scientific thermo-shaker. Afterward, we filtered the mixture through a Whatman No. 4 filter paper, discarded the solid, and used the filtered liquid for nanocomposite preparation.

2.4 Preparation of AgNPs/GO

For the biosynthesis of the AgNPs/GO nanocomposites, three different volumetric ratios consisting of graphene oxide, an aqueous extract of *Tamarix gallica*, and 5 mM AgNO_3 were used (1:1:1, 5:1:1, and 10:1:1). The precursor salt was added dropwise and kept under constant stirring (6

STIR) at room temperature until a change in color to dark brown. UV–Vis spectroscopy verified the formation of the AgNPs/GO nanocomposites. The nanosolids obtained were recovered by centrifugation at 12,000 rpm for 20 min and washed multiple times with deionized water.

2.5 Characterization

To analyze the nanomaterials, we used various methods, including ultraviolet–visible spectroscopy (Perkin Elmer Lambda 35), scanning electron microscopy (Schottky JEOL JSM-7600F), scanning transmission electron microscopy (Hitachi SU8230), X-ray diffraction (Bruker D8-Advance Lynx eye), and Fourier-transform infrared spectroscopy (Bruker Tensor 28). Additionally, we determined the concentration of Ag reduced for forming AgNPs deposited on rGO to form the Ag/rGO nanocomposite using atomic absorption spectroscopy (Perkin Elmer 3100).

2.6 Antibacterial activity

The disk diffusion method (Kirby–Bauer) determines the effectiveness of nanocomposites against two bacterial strains (*Escherichia coli* ATCC 25922 and *Staphylococcus aureus* ATCC 29213). The strains were cultured on Muller–Hinton agar using the cross-streak technique for 24 h at 37 °C, the ideal temperature for bacterial growth. The bacterial suspension was prepared in 15 mL of 4% saline solution and adjusted to McFarland standards for turbidity. The prepared bacteria solution was then seeded on Müller–Hinton agar. Sensi-disks were impregnated with different solutions, including sterile deionized water (negative control), erythromycin (positive control), AgNO₃, aqueous extract of *Tamarix gallica*, GO, and the AgNPs/GO nanocomposite used at varying concentrations (37.5, 75, 150, and 300 µg/mL). The materials were dispersed in an ultrasonic bath using a Branson 1510 ultrasound for 30 min as the dispersion degree of nanomaterial synthesized can affect their antibacterial activity. Finally, they were incubated at 37 °C for 48 h. This experiment was performed in triplicate.

3 Results and discussion

3.1 Preparation and characterization of AgNPs/GO

Scanning electron microscopy elucidates the morphology difference between graphite and GO. In Fig. 1a–b, graphite can be seen with micrometric sizes and thick layers. In contrast, Fig. 1b displays GO with a rough texture and distinct edges and folds resulting from oxygen-containing functional groups. These groups are obtained during the oxidation of

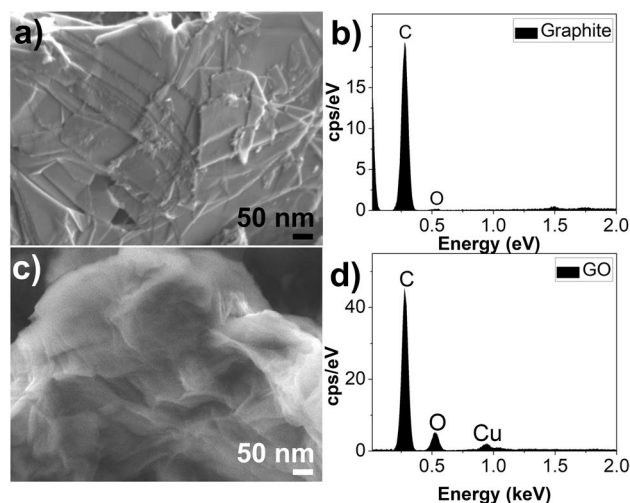


Fig. 1 SEM images and EDS chemical analysis of **a, b** graphite and **c, d** GO, respectively

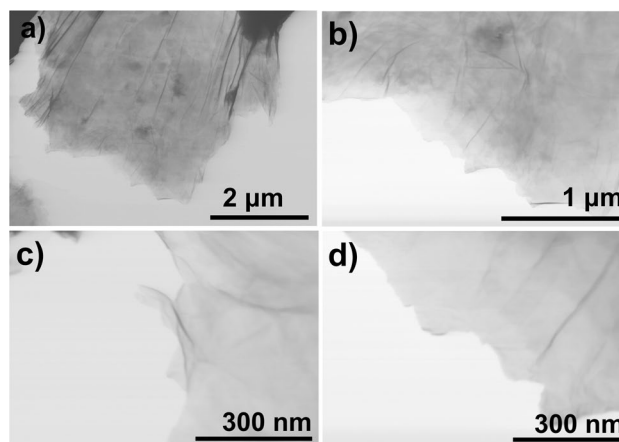


Fig. 2 BF-STEM images of GO nanosheets

graphite and subsequent cleavage in water, like the result reported by Jin et al. [21].

Chemical analysis of graphite and GO can be seen in Fig. 1c and d, respectively. Both spectra indicate the presence of carbon and oxygen signals. However, the GO spectrum displays a more prominent O signal, confirming the synthesis of this nanomaterial via graphite oxidation. Lastly, the copper signal is attributed to the sample holder.

It was used Bright-field scanning transmission electron microscopy (BF-STEM) to examine the physical characteristics of GO. The images in Fig. 2a, b show the layers of GO, in which the contrast difference can be distinguished between the center and edge of the particle. Figure 2b highlights the presence of edges and folds on the surface. To further examine the GO layers, we enlarged the image in Fig. 2a and obtained Fig. 2c. The transparent nanosheets

have a size of approximately 4.9 μm . We compared this film size to the average size measured in a centrifugal automatic particle analyzer, which was found to be 4.62 μm , a very similar result to that obtained by BF-STEM.

In Fig. 3a, the UV–Vis absorption spectrum of GO is shown, with bands at 222 and 300 nm. The first band corresponds to the π – π^* transitions of C=C aromatic bonds, and the second to the n – π^* transitions of C=O bonds [22]. Figure 3b displays the UV–Vis spectra of AgNPs/rGO for three different volumetric ratios of GO/aqueous extract/AgNO₃. The spectra show a redshift band attributed to GO reduction located at 285 nm [23]. Another band attributed to the surface plasmon resonance (SPR) of the AgNPs appears at 437 nm [24, 25]. As the proportion of GO increases, the intensity of the AgNPs band decreases due to more surface area where AgNPs nucleate and grow. Additionally, the GO band disappears, indicating its reduction. These results demonstrate how *Tamarix gallica* leaves and flowers' aqueous extract reduce GO and Ag to obtain the Ag/rGO nanocomposite.

In the study by Ksouri et al. [19], various phenolics and flavonoids were found in the water extract of *Tamarix gallica*, including its leaves and flowers that serve as the primary agents for reducing and stability of nanoparticles. It has been reported that the phenolic compounds present in the extracts act as the main precursors for the formation and stability of nanoparticles [26] due to the presence of hydroxyl groups (–OH) in their chemical structures that can

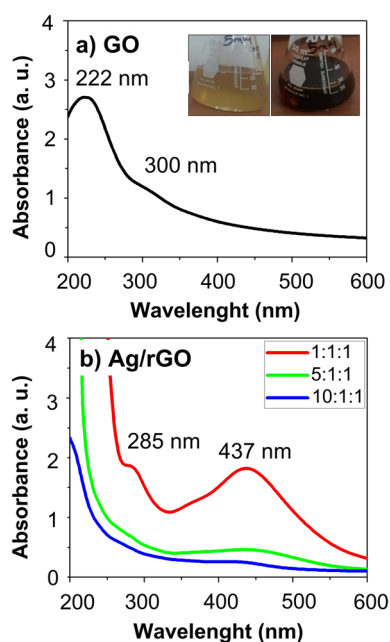


Fig. 3 UV–Vis absorption spectra of **a** GO and **b** AgNPs/GO nanocomposites for three different GO/aqueous extract/AgNO₃ volumetric ratios. Insert photographs of color change from slightly yellow to dark brown

donate electrons easily and reduce Ag⁺ ions and GO to form AgNPs and rGO simultaneously.

The crystal structure of the AgNPs/GO material was determined through XRD analyses. In Fig. 4a, the XRD pattern of graphite is shown with a prominent peak at $2\theta = 26.4^\circ$, corresponding to the interplanar distance of 3.38 Å of the (002) planes of the carbon hexagonal structure. Figure 4b displays the XRD pattern of GO, which only has one broadened peak located at $2\theta = 10.4^\circ$. This peak represents the interplanar distance of 8.50 Å. It is due to the insertion of various oxygenated functional groups (carbonyl, carboxyl, hydroxyl, epoxy, and ether) by the oxidation of graphite and exfoliation [27]. The broadening of the (002) planes from 0.38 to 1.22° indicates the formation of GO.

The Debye–Scherrer equation was used to determine the average crystallite size, resulting in a value of 6.5 nm. The average number of graphene layers and their derivatives (N) can be calculated using the peak amplification method and combining the Debye–Scherrer and Bragg equations. The expression for N is as follows [28]:

$$N = 1 + D/d \quad (1)$$

Here, D represents the average crystal size, and d represents the interplanar distance. The number of layers of the synthesized GO was 9, which is lower than the number obtained by Saini et al. [28], who used the modified Hummer's method ($N = 17$).

The XRD pattern for the AgNPs/rGO nanocomposite (Fig. 4c) revealed peaks at $2\theta = 38.16^\circ$, 44.65° , 64.41° , and 77.21° . These peaks corresponded to planes (111), (200), (220), and (311), respectively, of the face-centered cubic crystal structure (fcc) of Ag (standard data JCPDS No. 99-101-3078). However, the GO phase was not identified due to the differences in X-ray scattering factors between the AgNPs and rGO [29, 30]. Instead, the XRD pattern showed additional peaks related to the organic compounds that remained in the extract, which were responsible for

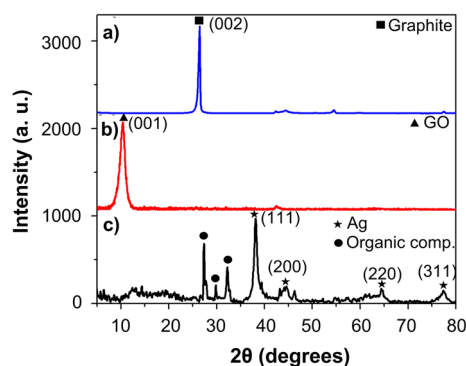


Fig. 4 XRD patterns of **a** graphite, **b** GO, and **c** AgNPs/GO nanocomposite

stabilizing the AgNPs. These compounds are known to be difficult to identify. Based on the Debye–Scherrer equation, the average crystallite size of the AgNPs deposited in the 2D nanomaterial was 35 nm.

BF-STEM performed the morphological and chemical characterizations of the AgNPs/GO nanocomposite.

Figure 5a shows a secondary electron (SE) SEM image exhibiting the deposition of AgNPs dispersed on the nanolayer's surface. Figure 5b displays a BF-STEM image showing spherical and semispherical AgNPs on rGO. Figure 5c illustrates a dark-field (DF) STEM image, where the contrast is related to the atomic number of the elements (Z contrast). This image clearly shows the AgNPs deposited on GO. Also, Fig. 5d shows BF-STEM and SE images superposition, where AgNPs in the 5–40 nm range and the rGO thickness are observed. Smaller AgNPs sizes are essential for antibacterial applications [31, 32]. Also, spherical nanoparticles have better antibacterial activity [33–35]. Finally, the chemical composition of the nanocomposite was confirmed by EDS spectroscopy. Figure 6e shows its corresponding spectra, illustrating the presence of the C, O, and Ag elements contained in the nanocomposite.

The AgNPs/GO nanocomposite underwent morphological and chemical characterizations by BF-STEM. The STEM technique uses transmitted electrons and works best with

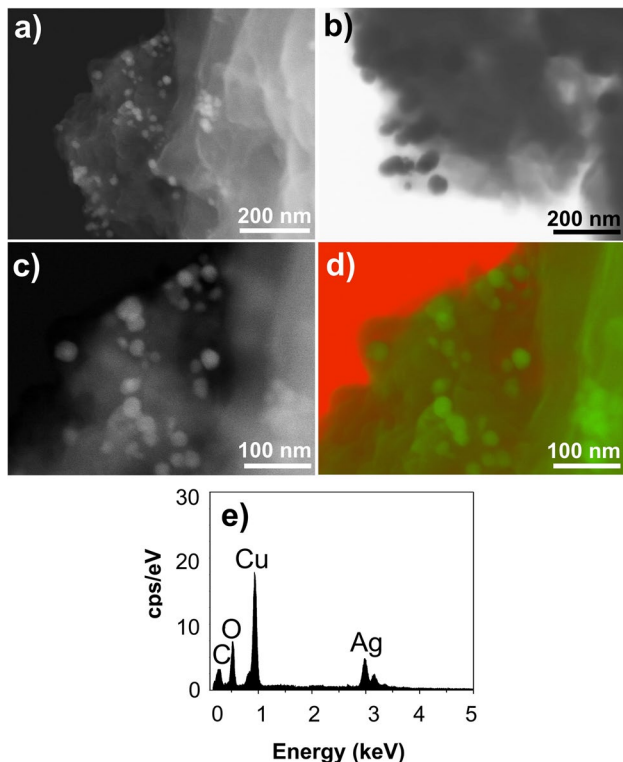


Fig. 5 AgNPs/GO nanocomposite SEM micrographs, **a** SE, **b** BF-STEM, **c** DF-STEM, **d** BF-STEM + SE, and **e** EDS chemical analysis

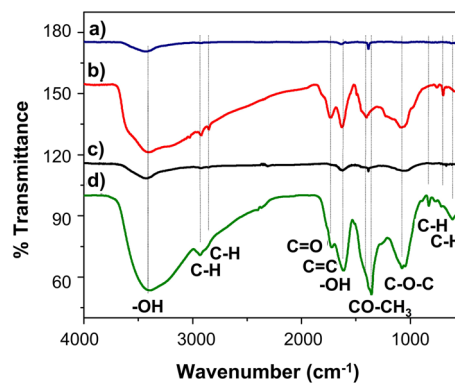


Fig. 6 FT-IR spectra. **a** graphite, **b** GO, **c** AgNPs/GO nanocomposite, and **d** *Tamarix gallica* aqueous extract

thin samples like graphene oxide, allowing higher-quality imaging. However, thicker samples like graphite do not qualify for transparency and will appear very dark in images. In Fig. 5a a secondary electron SEM image shows the deposition of AgNPs dispersed on the surface of the nanolayer. Meanwhile, Fig. 5b displays a BF-STEM image that exhibits spherical and semispherical AgNPs on rGO. The dark-field (DF) STEM image in Fig. 5c illustrates the AgNPs deposited on GO, with the contrast related to the atomic number of the elements (Z contrast). In Fig. 5d, the BF-STEM and SE images are superimposed, revealing AgNPs in the 5–40 nm range and the thickness of rGO.

Smaller AgNPs sizes are crucial for antibacterial applications, and spherical nanoparticles have good antibacterial activity [31–35]. Finally, the nanocomposite's chemical composition was confirmed by EDS spectroscopy, as shown in Fig. 6e's corresponding spectra that illustrate the presence of C, O, and Ag elements. Similar sizes have been obtained by other researchers using different methods.

The different materials were studied using FT-IR spectroscopy to identify their functional groups. Figure 6a displayed the graphite spectrum, which showed three absorption bands at 3426 cm^{-1} , 1642 cm^{-1} , and 1381 cm^{-1} . These correspond to the functional groups –OH (alcohols/water), C=C (aromatic compounds), and –OH (carboxylic acids).

Figure 6b shows the GO spectrum with bands centered at 3446 cm^{-1} , 2921 cm^{-1} , 2850 cm^{-1} , 1728 cm^{-1} , 1627 cm^{-1} , 1402 cm^{-1} , 1081 cm^{-1} , and 755 cm^{-1} . These bands correspond to the functional groups –OH (alcohols/water), C–H (alkanes), C–H (alkanes), C=O (carboxylic acids), C=C (aromatic compounds), –OH (carboxylic acids), C–O–C (ethers), and C–H (aromatic compounds), respectively. The insertion of various oxygenated functional groups is attributed to graphite oxidation and subsequent water exfoliation, confirming the GO synthesis [36–38].

The FT-IR spectrum of the AgNPs/GO nanocomposite is shown in Fig. 6c. The FT-IR spectrum of GO reveals

bands at 3446 cm^{-1} , 1402 cm^{-1} , and 1081 cm^{-1} , which correspond to the functional groups $-\text{OH}$, $-\text{OH}$, and $\text{C}-\text{O}-\text{C}$, respectively. Also, the peak at 1078 cm^{-1} corresponding to the carbonyl functional group ($\text{C}=\text{O}$) disappeared. These bands decreased their intensity, corroborating GO's reduction. These results are consistent with those obtained from UV-Vis spectroscopy. Other studies have also observed similar results using L-methionine [39], *Pistacia atlantica* [15], and sodium citrate [40] as reducing and stabilizing agents.

Besides, Fig. 6d shows the FT-IR spectrum of the aqueous extract of *Tamarix gallica* showing bands located at 3390 cm^{-1} , 2930 cm^{-1} , 1612 cm^{-1} , 1355 cm^{-1} , 1075 cm^{-1} , and 840 cm^{-1} ; these bands correspond to the following functional groups, $-\text{OH}$ (alcohols), $\text{C}-\text{H}$ (alkanes), $\text{C}=\text{C}$ (aromatic compounds), $\text{CO}-\text{CH}_3$ (benzenes), the latter associated with aromatic compounds [18], $\text{C}-\text{O}$ (alcohols) and $\text{C}-\text{H}$ (aromatic compounds), respectively. All functional groups can be related to various phenolic compounds, which consist of at least one phenol. That is correspond, a hydroxylated aromatic ring: tannins (gallic and ellagic acid) [41, 42] and flavonoids, such as quercetin 3-O-glucuronide, quercetin, kaempferol, rhamnocitrin, flavone, catechin, epicatechin, amentoflavone, apigenin, and resveratrol 3-O-glucoside [42].

All characterization techniques confirmed the successful simultaneous synthesis of AgNPs and reduction of GO to form an Ag/rGO nanocomposite in a single step using *Tamarix gallica* aqueous extract (leaves and flowers).

Through all characterization techniques, it has been confirmed that the synthesis of AgNPs and reduction of GO occurred simultaneously in a single step using *Tamarix gallica* aqueous extract (leaves and flowers), forming an Ag/rGO nanocomposite.

3.2 Antibacterial activity

In Fig. 7a–h, the antibacterial activity against *E. coli* and *S. aureus* ATCC 29213 was tested using GO, AgNPs/rGO, deionized water, aqueous extract of *T. gallica*, AgNO_3 , and an antibiotic (erythromycin). At concentrations of $37.5\text{ }\mu\text{g/mL}$, $75\text{ }\mu\text{g/mL}$, and $150\text{ }\mu\text{g/mL}$, no inhibition halos were observed in the nanomaterials shown in Fig. 7a–c and e–g. Additionally, the deionized water, aqueous extract of *T. gallica*, GO, and AgNO_3 did not exhibit inhibition halos for either of the tested microorganisms. Ksouri et al. [19] reported that the aqueous extract of *Tamarix gallica* leaves and flowers had antibacterial activity against both *E. coli* and *S. aureus*, starting from concentrations of 0.146 mg/mL . However, the extract concentration used in this study was lower than the MIC concentration used by Ksouri [19]. These results are consistent with Thomas et al. [43], who observed no inhibition halo against *S. aureus* using $40\text{ }\mu\text{L}$ of AgNO_3 (1 mM), with an Ag concentration of $107.9\text{ }\mu\text{g/mL}$, which also did not show an inhibition halo for either bacterium.

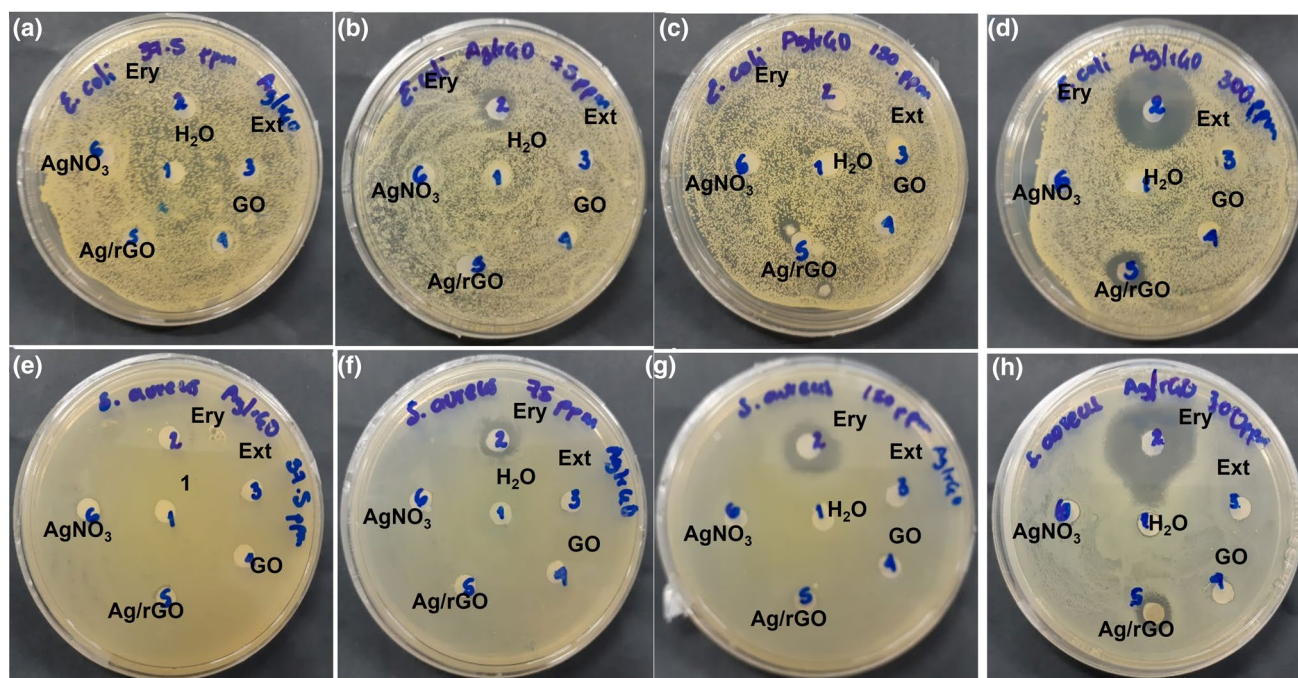


Fig. 7 The antibacterial activity against **a–d** *E. coli* and **e–h** *S. aureus* tested for 1-deionized water, 2-erythromycin, 3-*T. gallica* aqueous extract, 4-GO, 5-Ag/rGO, and 6- AgNO_3 using concentrations from left to right of 37 ppm, 75 ppm, 150 ppm, and 300 ppm, respectively

In Fig. 7d and e, both bacteria show a clear inhibition halo at 300 $\mu\text{g/mL}$ of AgNPs/GO. This concentration is considered the minimum inhibition concentration (MIC).

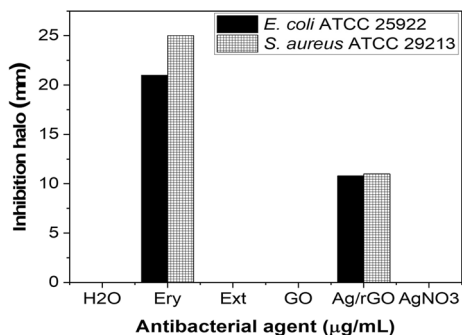


Fig. 8 Bar graph of measurements of inhibition halos for **a** *E. coli* and **b** *S. aureus*

In Fig. 8, the bar graph displays the inhibition halos for the two selected strains. At 300 $\mu\text{g/mL}$ concentration, the inhibition radius was 10.8 mm for *E. coli* and 11 mm for *S. aureus*. The higher sensitivity of Gram-negative *S. aureus* is due to its lack of an outer membrane, which makes it more vulnerable to AgNPs/rGO attack. In contrast, Gram-positive *E. coli* has three layers: an outer membrane, a peptidoglycan cell wall, and an inner membrane [44].

This investigation compared the results obtained with previous reports (Table 1). The inhibition concentration of the synthesized nanocomposites was found to be lower than those made with *Pistacia atlantica* leaf extract [15], *Pseudomonas aeruginosa* biomass extract [45], bitter gourd leaf extract [46], and by pulsed laser ablation [47] against the same bacterium. However, Barúa et al. [48] reported growth inhibition of *E. coli* and *S. aureus* of 20 and 12.5 ppm, respectively, using five times more doses than in the present study. Rajeswari et al. [49] and Prasad et al. [50] have also

Table 1 Comparison of Ag/rGO nanocomposite's antibacterial effect against *E. coli* and *S. aureus* in different studies

Nano-composite	Synthesis method/ reducing and stabiliz- ing agent	Bacteria	Particle morphology/ size (nm)	Conc (ppm)	Dosage (μL)	Inhibition halo (mm)
Ag/rGO [1]	Green/ <i>Pistacia atlantica</i> leaves extract	<i>E. coli</i> ATCC 25922 <i>S. aureus</i> ATCC 25923	Spherical 13–73	1000	60	18.8 \pm 0.44 20.0 \pm 0.7
Ag/rGO [2]	Green/ <i>Colocasia esculenta</i> leaf extract	<i>E. coli</i> ATCC 10536 <i>S. aureus</i> ATCC 11632	Spherical 5–25	20 12.5	50	18.84 \pm 0.06 23.82 \pm 0.18
Ag/rGO [3]	Green/ <i>Averrhoa carambola</i> leaf extract	<i>E. coli</i> MTCC 433 <i>S. aureus</i> MTCC 737	Cubic 90–120	–	20 mg	25.0 \pm 2.0 30.0 \pm 3.0
Ag/rGO [4]	Green/Naringenin	<i>E. coli</i> MTCC 1687 <i>S. aureus</i> MTCC 96	Spherical 6–28	–	25	10.0 9.0
Ag/GO [5]	Green/ <i>Pseudomonas aeruginosa</i> biomass extract	<i>E. coli</i> <i>S. aureus</i>	Spherical 22–42	5000	–	20.0 \pm 0.29 16.0 \pm 0.32
Ag@AgCl/rGO [6]	Green/Bitter gourd leaf extract	<i>E. coli</i> <i>S. aureus</i>	Spherical 40	1000	–	7.0 4.5
Ag/rGO [7]	Hydro-thermal	<i>E. coli</i> ATCC 23848 <i>S. aureus</i> ATCC 25923	Spherical 21	100	–	18.0 8.0
Ag/rGO [8]	Chemical and thermal/ sodium potassium tartrate and poly vinyl pyrrolidone (PVP)	<i>E. coli</i> <i>S. aureus</i>	Spherical 1–15	100	–	25.0 \pm 2.0 24.0 \pm 1.0
Ag/GO [9]	Pulsed laser ablation	<i>E. coli</i> <i>S. aureus</i>	Spherical 5–30	5000	–	10.2 \pm 1.1 15.2 \pm 1.6
Ag/rGO [10]	Green/Glucose	<i>E. coli</i> <i>S. aureus</i>	Spherical 50	–	50	23.7 \pm 0.8 21.0 \pm 2.2
Ag/rGO This research	Green/ <i>Tamarix gallica</i> aqueous extract	<i>E. coli</i> ATCC 25922 <i>S. aureus</i> ATCC 29213	Spherical and semi-spherical 5–40	300	10	10.8 11.0

reported inhibition halos for the same microorganisms, but the latter did not specify the amount used.

Previous research has identified several factors that strongly impact the antibacterial properties of this nanomaterial, including the number of layers and size of the nanosheets [51]. As the number of GO or rGO layers increases, the material becomes less dispersible and more prone to aggregation, resulting in reduced contact with microorganisms [51].

In this study, XRD results revealed that there were 9 GO layers present, which is responsible for the decreased antibacterial activity in GO. Aunkor et al. [52] found that the MIC against *E. coli* and *S. aureus* for the GO monolayer was 65 µg/ml due to the sharp edges of the GO, which can act like "nano knives" and penetrate the cell wall and membrane, causing damage to the cell. This concentration was lower than that reported in this work.

Yu et al. [53] researched GO monolayers using AFM results. The relationship between GO layer size and antibacterial activity is unclear. When tested with different sizes of GO (25 µg/mL), bacterial viability showed different values of 57%, 78%, 41%, and 35% for sizes of 1295 nm, 2015 nm, 3074 nm, and 4544 nm, respectively. However, the last size of GO used in their study, like the size used in this work, confirmed its antibacterial effect. Other factors, such as nanoparticle size, may also influence the size of bacterial Ag/rGO inhibition halos. Smaller nanoparticle sizes tend to have a better bactericidal effect [33].

One important factor is the spherical shape of the nanomaterial, which has been shown to inhibit bacterial growth effectively [34]. The concentration and dosage of the material also play a role in its effectiveness. A synergistic antibacterial effect between AgNPs and GO-film was expected. However, the results did not demonstrate stronger antibacterial activity for AgNPs/rGO than previous studies on AgNPs. These findings suggest that the larger surface area of AgNPs without GO acts more effectively on the bacterial membrane by fighting bacteria [54]. However, the AgNPs incorporated into the rGO nanofilm can be useful as a surface coating, distribute evenly throughout the film, and can be deposited on various surfaces. These findings align with previous research and suggest potential biomedical applications for this nanomaterial in the future.

4 Conclusions

We successfully used an aqueous extract of *Tamarix gallica* to build a nanocomposite of AgNPs and GO through co-reduction. The Kirby-Bauer method was used to measure the antibacterial activity of the nanocomposite. At the same time, its morphological, structural, and chemical characteristics were determined through UV–Vis, SEM,

STEM, XRD, and FT-IR techniques. UV–Vis spectroscopy confirmed GO formation through the electronic transition bands $\pi-\pi^*$ and $n-\pi^*$, corresponding to the C=C and C=O bonds. The formation of the AgNPs/GO nanocomposite was determined by the characteristic UV–Vis bands for rGO and AgNPs (SPR). SEM/STEM analyses showed the successful deposition of semispherical AgNPs ranging in size from 5 to 40 nm in the rGO. XRD revealed crystal structures of GO (hcp) and Ag (fcc). Additionally, FT-IR spectroscopy confirmed the decrease in oxygenated functional groups (C=O, C–O–C, –OH) present in GO after bioreduction using the aqueous extract of *Tamarix gallica*. The antibacterial tests on AgNPs/GO showed growth inhibition in bacteria *E. coli* and *S. aureus*.

Author contributions All authors contributed to the study conception and design. AH-R performed the methodology, analysis, and investigation. RE and JCG-H checked the supervision and GR checked the supervision, writing, review, and editing. All authors read and approved the final manuscript.

Funding Not applicable.

Availability of data and materials All data analyzed during this study are included in the article.

Declarations

Conflict of interest The authors declare that they have no conflict of interest.

References

1. K.-S. Novoselov, A.-K. Geim, S.-V. Morozov, D. Jiang, Y. Zhang, S.-V. Dubonos, I.-V. Grigorieva, A.-A. Firsov, Electric field effect in atomically thin carbon films. *Science* **306**, 666–669 (2004). <https://doi.org/10.1126/science.1102896>
2. G. Yang, L. Li, W.-B. Lee, M.-C. Ng, Structure of graphene and its disorders: a review. *Sci. Technol. Adv. Mater.* **19**, 613–648 (2018). <https://doi.org/10.1080/14686996.2018.1494493>
3. M. Tahriri, M. Del Monaco, A. Moghanian, M. TavakkoliYaraki, R. Torres, A. Yadegari, L. Tayebi, Graphene and its derivatives: opportunities and challenges in dentistry. *Mater. Sci. Eng. C* **102**, 171–185 (2019). <https://doi.org/10.1016/j.msec.2019.04.051>
4. A.-G. Olabi, M.-A. Abdelkareem, T. Wilberforce, E.-T. Sayed, Application of graphene in energy storage device – a review. *Renew. Sustain. Energy Rev.* **135**, 110026 (2021). <https://doi.org/10.1016/j.rser.2020.110026>
5. S.-S. Ashok Sharma, S. Bashir, R. Kasi, R.-T. Subramaniam, The significance of graphene based composite hydrogels as smart materials: a review on the fabrication, properties, and its applications. *FlatChem* **33**, 100352 (2022). <https://doi.org/10.1016/j.flatc.2022.100352>
6. A.-M. Díez-Pascual, Antibacterial action of nanoparticle loaded nanocomposites based on graphene and its derivatives: a mini-review. *Int. J. Mol. Sci.* **21**, 3563 (2020). <https://doi.org/10.3390/ijms21103563>
7. A. Khezerlou, M. Alizadeh-Sani, M. Azizi-Lalabadi, A. Ehsani, Nanoparticles and their antimicrobial properties against pathogens

- including bacteria, fungi, parasites and viruses. *Microb. Pathog. Pathog.* **123**, 505–526 (2018). <https://doi.org/10.1016/j.micpath.2018.08.008>
8. C. Bankier, R.-K. Matharu, Y.-K. Cheong, G.-G. Ren, E. Cloutman-Green, L. Ciric, Synergistic antibacterial effects of metallic nanoparticle combinations. *Sci. Rep.* **9**, 1–8 (2019). <https://doi.org/10.1038/s41598-019-52473-2>
 9. C. Aydin Acar, S. Pehlivanoglu, Ş Yeşilot, S. Uzuner, Microwave-assisted biofabrication of silver nanoparticles using *Helichrysum arenarium* flower extract: characterization and biomedical applications. *Biomass Convers. Biorefin.* (2023). <https://doi.org/10.1007/s13399-023-03833-6>
 10. Y. Li, Q. Song, B. Fan, R. Zhang, Effects of reducing agents on the synthesis of Ag/rGO nanocomposites. *Mater. Res. Express.* **4**, 015014 (2017). <https://doi.org/10.1088/2053-1591/aa522e>
 11. C. He, Z. Liu, Y. Lu, L. Huang, Y. Yang, Graphene-supported silver nanoparticles with high activities toward chemical catalytic reduction of methylene blue and electrocatalytic oxidation of hydrazine. *Int. J. Electrochem. Sci. Electrochem. Sci.* **11**, 9566–9574 (2016). <https://doi.org/10.20964/2016.11.72>
 12. Z. Çiplak, N. Yıldız, A. Çalimli, Investigation of graphene/Ag nanocomposites synthesis parameters for two different synthesis methods. *Fuller. Nanotub. Carbon Nanostruct.* **23**, 361–370 (2015). <https://doi.org/10.1080/1536383X.2014.894025>
 13. C.-P. Devatha, A.-K. Thalla, *Green Synthesis of Nanomaterials* (W. Publishing, 2018), pp. 169–184
 14. M.-A. Malik, A.-A. Alshehri, R. Patel, Facile one-pot green synthesis of Ag–Fe bimetallic nanoparticles and their catalytic capability for 4-nitrophenol reduction. *J. Mater. Res. Technol.* **12**, 455–470 (2021). <https://doi.org/10.1016/j.jmrt.2021.02.063>
 15. H. Veisi, M. Kavian, M. Hekmati, S. Hemmati, Biosynthesis of the silver nanoparticles on the graphene oxide's surface using *Pistacia atlantica* leaves extract and its antibacterial activity against some human pathogens. *Polyhedron* **161**, 338–345 (2019). <https://doi.org/10.1016/j.poly.2019.01.034>
 16. A.-R. Soleymani, S.-M. Rafigh, M. Hekmati, Green synthesis of RGO/Ag: As evidence for the production of uniform mono-dispersed nanospheres using microfluidization. *Appl. Surf. Sci.* **518**, 146264 (2020). <https://doi.org/10.1016/j.apsusc.2020.146264>
 17. M. Cobos, I. De-La-Pinta, G. Quindós, M.-J. Fernández, M.-D. Fernández, Graphene oxide–silver nanoparticle nanohybrids: Synthesis, characterization, and antimicrobial properties. *Nanomaterials* **10**, 376 (2020). <https://doi.org/10.3390/nano10020376>
 18. J.-L. López-Miranda, M. Vázquez, N. Fletes, R. Esparza, G. Rosas, Biosynthesis of silver nanoparticles using a *Tamarix gallica* leaf extract and their antibacterial activity. *Mater. Lett.* **176**, 285–289 (2016). <https://doi.org/10.1016/j.matlet.2016.04.126>
 19. R. Ksouri, H. Falleh, W. Megdiche, N. Trabelsi, B. Mhamdi, K. Chaieb, A. Bakrouf, C. Magné, C. Abdely, Antioxidant and antimicrobial activities of the edible medicinal halophyte *Tamarix gallica* L. and related polyphenolic constituents. *Food Chem. Toxicol.* **47**, 2083–2091 (2009). <https://doi.org/10.1016/j.fct.2009.05.040>
 20. D.-C. Marcano, D.-V. Kosynkin, J.-M. Berlin, A. Sinitkii, Z. Sun, A. Slesarev, L.-B. Alemany, W. Lu, J.-M. Tour, Improved synthesis of graphene oxide. *ACS Nano* **4**, 4806–4814 (2010). <https://doi.org/10.1021/nn1006368>
 21. X. Jin, N. Li, X. Weng, C. Li, Z. Chen, Green reduction of graphene oxide using Eucalyptus leaf extract and its application to remove dye. *Chemosphere* **208**, 417–424 (2018). <https://doi.org/10.1016/j.chemosphere.2018.05.199>
 22. M. Nasrollahzadeh, S.-M. Sajadi, M. Maham, *Tamarix gallica* leaf extract mediated novel route for green synthesis of CuO nanoparticles and their application for N-arylation of nitrogen-containing heterocycles under ligand-free conditions. *RSC Adv.* **5**, 40628–40635 (2015). <https://doi.org/10.1039/C5RA04012D>
 23. R. Geetha Bai, K. Muthoosamy, F. Shipton, A. Pandikumar, P. Kumar, H. Ming, S. Manickam, The biogenic synthesis of reduced graphene oxide–silver (RGO–Ag) nanocomposite and its dual applications as antibacterial agent and cancer biomarker sensor. *RSC Adv.* **6**, 36576–36587 (2016). <https://doi.org/10.1039/C6RA02928K>
 24. R. Shanmuganathan, G. Sathishkumar, K. Brindhadevi, A. Pugazhendhi, Fabrication of naringenin functionalized-Ag/RGO nanocomposites for potential bactericidal effects. *J. Mater. Res. Technol.* **9**, 7013–7019 (2020). <https://doi.org/10.1016/j.jmrt.2020.03.118>
 25. S. Hemmati, M.-M. Heravi, B. Karmakar, H. Veisi, Green fabrication of reduced graphene oxide decorated with Ag nanoparticles (rGO/Ag NPs) nanocomposite: a reusable catalyst for the degradation of environmental pollutants in aqueous medium. *J. Mol. Liq.* **319**, 114302 (2020). <https://doi.org/10.1016/j.molliq.2020.114302>
 26. C. Devatha, A.K. Thalla, S.-Y. Katte, Green synthesis of iron nanoparticles using different leaf extracts for treatment of domestic waste water. *J. Clean. Prod.* **139**, 1425–1435 (2016). <https://doi.org/10.1016/j.jclepro.2016.09.019>
 27. K.-S. Divya, V.-N. Reethu, S. Mathew, Enhanced photocatalytic performance of RGO/Ag nanocomposites produced via a facile microwave irradiation for the degradation of Rhodamine B in aqueous solution. *Appl. Surf. Sci.* **444**, 811–818 (2018). <https://doi.org/10.1016/j.apsusc.2018.01.303>
 28. P. Saini, R. Sharma, N. Chadha, Determination of defect density, crystallite size and number of graphene layers in graphene analogues using X-ray diffraction and Raman spectroscopy. *Indian J. Pure Appl. Phys.* **55**, 625–629 (2017)
 29. C. Xu, X. Wang, J. Zhu, Graphene–metal particle nanocomposites. *J. Phys. Chem. C* **112**, 19841–19845 (2008). <https://doi.org/10.1021/jp807989b>
 30. C. Xu, X. Wang, Fabrication of flexible metal-nanoparticle films using graphene oxide sheets as substrates. *Small* **5**, 2212–2217 (2009). <https://doi.org/10.1002/sml.200900548>
 31. S.-P. Nayak, S.-S. Ramamurthy, J.-K. Kiran Kumar, Green synthesis of silver nanoparticles decorated reduced graphene oxide nanocomposite as an electrocatalytic platform for the simultaneous detection of dopamine and uric acid. *Mater. Chem. Phys.* **252**, 123302 (2020). <https://doi.org/10.1016/j.matchemphys.2020.123302>
 32. J. Wu, B. Zhu, Y. Zhao, M. Shi, X. He, H. Xu, Q. Zhou, One-step eco-friendly synthesis of Ag-reduced graphene oxide nanocomposites for antibiofilm application. *J. Mater. Eng. Perform.* **29**, 2551–2559 (2020). <https://doi.org/10.1007/s11665-020-04742-9>
 33. Y. Dong, H. Zhu, Y. Shen, W. Zhang, L. Zhang, Antibacterial activity of silver nanoparticles of different particle size against *Vibrio natriegens*. *PLoS ONE* **14**, 1–12 (2019). <https://doi.org/10.1371/journal.pone.0222322.g006>
 34. M.-A. Raza, Z. Kanwal, A. Rauf, A.-N. Sabri, S. Riaz, S. Naseem, Size- and shape-dependent antibacterial studies of silver nanoparticles synthesized by wet chemical routes. *Nanomaterials* **6**, 74 (2016). <https://doi.org/10.3390/nano6040074>
 35. J.-Y. Cheon, S.-J. Kim, Y.-H. Rhee, O.-H. Kwon, W.-H. Park, Shape-dependent antimicrobial activities of silver nanoparticles. *Int. J. Nanomed. Nanomed.* **14**, 2773–2780 (2019). <https://doi.org/10.2147/IJN.S196472>
 36. R. Aradhana, S. Mohanty, S. Nayak, Comparison of mechanical, electrical and thermal properties in graphene oxide and reduced graphene oxide filled epoxy nanocomposite adhesives. *Polym. J.* **141**, 109–123 (2018). <https://doi.org/10.1016/j.polymer.2018.03.005>
 37. M. Bera, C. Yadav, P. Gupta, P. Maji, Facile one-pot synthesis of graphene oxide by sonication assisted mechanochemical approach and its surface chemistry. *J. Nanosci. Nanotechnol.* **14**, 1–12 (2013). <https://doi.org/10.1002/jnn.22400>

- Nanotechnol. **18**, 902–912 (2018). <https://doi.org/10.1166/jnn.2018.14306>
38. N. Bandara, Y. Esparza, J. Wu, Graphite oxide improves adhesion and water resistance of canola protein–graphite oxide hybrid adhesive. *Sci. Rep.* **7**, 1–12 (2017). <https://doi.org/10.1038/s41598-017-11966-8>
39. N. Belachew, D.-S. Meshesha, K. Basavaiah, Green syntheses of silver nanoparticle decorated reduced graphene oxide using L-methionine as a reducing and stabilizing agent for enhanced catalytic hydrogenation of 4-nitrophenol and antibacterial activity. *RSC Adv.* **9**, 39264–39271 (2019). <https://doi.org/10.1039/C9RA08536J>
40. M. Moghayedi, E.-K. Goharshadi, K. Ghazvini, H. Ahmadzadeh, L. Ranjbaran, R. Masoudi, R. Ludwig, Kinetics and mechanism of antibacterial activity and cytotoxicity of Ag-RGO nanocomposite. *Colloids Surf. B* **159**, 366–374 (2017). <https://doi.org/10.1016/j.colsurfb.2017.08.001>
41. A. Sehrawat, S. Sultana, *Tamarix gallica* ameliorates thioacetamide-induced hepatic oxidative stress and hyperproliferative response in Wistar rats. *J. Enzyme Inhib. Med. Chem.* **21**, 215–223 (2006). <https://doi.org/10.1080/14756360500480673>
42. M. Boulaaba, M. Snoussi, M. Saada, K. Mkadmini, A. Smaoui, C. Abdelly, R. Ksour, Antimicrobial activities and phytochemical analysis of *Tamarix gallica* extracts. *Ind. Crops Prod.* **76**, 1114–1122 (2015). <https://doi.org/10.1016/j.indcrop.2015.08.020>
43. R. Thomas, A. Janardhanan, R.-T. Varghese, E. Soniya, J. Mathew, E. Radhakrishnan, Antibacterial properties of silver nanoparticles synthesized by marine *Ochrobactrum* sp. *Braz. J. Microbiol. Microbiol.* **45**, 1221–1227 (2014). <https://doi.org/10.1590/s1517-83822014000400012>
44. Z. Breijyeh, B. Jubeh, R. Karaman, Resistance of Gram-negative bacteria to current antibacterial agents and approaches to resolve it. *Molecules* **25**, 1340 (2020). <https://doi.org/10.3390/molecules25061340>
45. A.-K. Potbhare, M.-S. Umekar, P.-B. Chouke, M.-B. Bagade, S.-T. Aziz, A.-A. Abdala, R.-G. Chaudhary, Bioinspired graphene-based silver nanoparticles: fabrication, characterization and antibacterial activity. *Mater. Today: Proc.* **29**, 720–725 (2020). <https://doi.org/10.1016/j.matpr.2020.04.212>
46. T.-B. Devi, M. Ahmaruzzaman, Facile synthesis of rGO/Ag@AgCl core-shells nanocomposite and their multifunctional efficacy as a photocatalyst and antimicrobial agent for decontamination of water. *J. Alloys Compd.* **860**, 157988 (2021). <https://doi.org/10.1016/j.jallcom.2020.157988>
47. A.-A. Menazea, M.-K. Ahmed, Silver and copper oxide nanoparticles-decorated graphene oxide via pulsed laser ablation technique: preparation, characterization, and photoactivated antibacterial activity. *Nano-Struct. Nano-Objects* **22**, 100464 (2020). <https://doi.org/10.1016/j.nanoso.2020.100464>
48. S. Barua, S. Thakur, L. Aidew, A.-K. Buragohain, P. Chattopadhyay, N. Karak, One step preparation of a biocompatible, antimicrobial reduced graphene oxide–silver nanohybrid as a topical antimicrobial agent. *RSC Adv.* **4**, 9777–9783 (2014). <https://doi.org/10.1039/C3RA46835F>
49. R. Rajeswari, H.-G. Prabu, D.-M. Amutha, One Pot Hydrothermal synthesis characterizations of silver nanoparticles on reduced graphene oxide for its enhanced antibacterial and antioxidant properties. *IOSR J. Appl. Chem.* **10**, 64–69 (2017). <https://doi.org/10.9790/5736-1005016469>
50. K. Prasad, G.-S. Lekshmi, K. Ostrikov, V. Lussini, J. Blinco, M. Mohandas, K. Vasilev, S. Bottle, K. Bazaka, K. Ostrikov, Synergic bactericidal effects of reduced graphene oxide and silver nanoparticles against Gram-positive and Gram-negative bacteria. *Sci. Rep.* **7**, 1591 (2017). <https://doi.org/10.1038/s41598-017-01669-5>
51. H. Mohammed, A. Kumar, E. Bekyarova, Y. Al-Hadeethi, X. Zhang, M. Chen, M.S. Ansari, A. Cochis, L. Rimondini, Antimicrobial mechanisms and effectiveness of graphene and graphene-functionalized biomaterials a scope review. *Front. Bioeng. Biotechnol.* **8**, 465 (2020). <https://doi.org/10.3389/fbioe.2020.00465>
52. M.-T.-H. Aunkor, T. Raihan, S.-H. Prodhon, H. Metselaar, S.-U.-F. Malik, A.-K. Azad, Antibacterial activity of graphene oxide nanosheet against multidrug resistant superbugs isolated from infected patients. *R. Soc. Open Sci.* **7**, 200640 (2020). <https://doi.org/10.1098/rsos.200640>
53. C.-H. Yu, G.-Y. Chen, M.-Y. Xia, Y. Xie, Y.-Q. Chi, Z.-Y. He, C.-L. Zhang, T. Zhang, Q.-M. Chen, Q. Peng, Understanding the sheet size-antibacterial activity relationship of graphene oxide and the nano-bio interaction-based physical mechanisms. *Colloids Surf. B Biointerfaces* **191**, 111009 (2020). <https://doi.org/10.1016/j.colsurfb.2020.111009>
54. S. Khorrami, Z. Abdollahi, G. Eshaghi, A. Khosravi, E. Bidram, A. Zarrabi, An improved method for fabrication of Ag–GO nanocomposite with controlled anti-cancer and anti-bacterial behavior. A comparative study. *Sci. Rep.* **9**, 9167 (2019). <https://doi.org/10.1038/s41598-019-45332-7>

Publisher's Note Springer Nature remains neutral with regard to jurisdictional claims in published maps and institutional affiliations.

Springer Nature or its licensor (e.g. a society or other partner) holds exclusive rights to this article under a publishing agreement with the author(s) or other rightsholder(s); author self-archiving of the accepted manuscript version of this article is solely governed by the terms of such publishing agreement and applicable law.